Supplementary Material for

Multi-decadal changes in Southern Ocean ventilation since the 1960s driven by wind and buoyancy forcing

Lavinia Patara, Claus W. Böning, Toste Tanhua

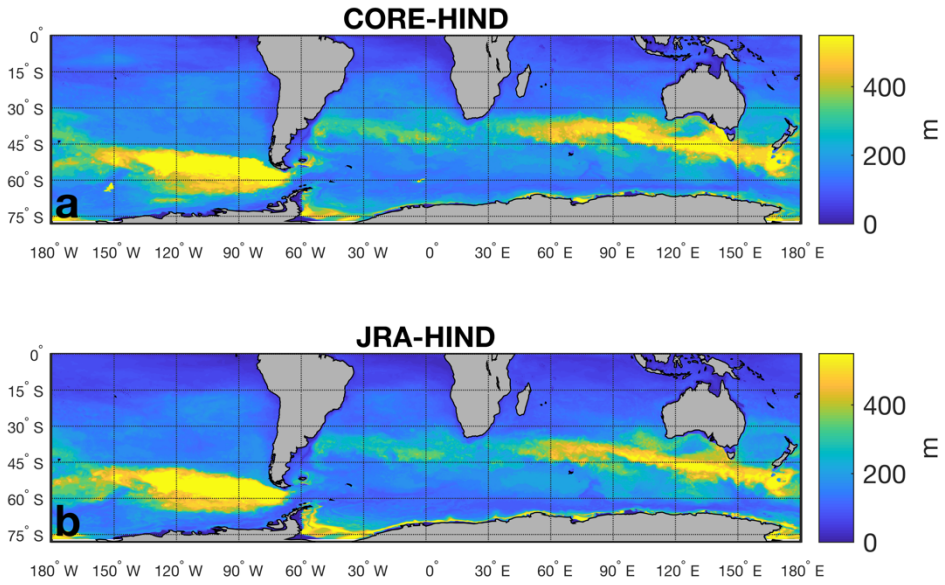

Fig. S1: Maximum MLD in the **a)** CORE experiments and in the **b)** JRA experiments calculated over the whole length of the simulations and over all experiments, i.e. **a)** 1948-2009 in CORE-CLIM, CORE-HIND, CORE-WIND and CORE-BUOY and **b)** 1958-2018 in JRA-CLIM1, JRA-CLIM2, and JRA-HIND.

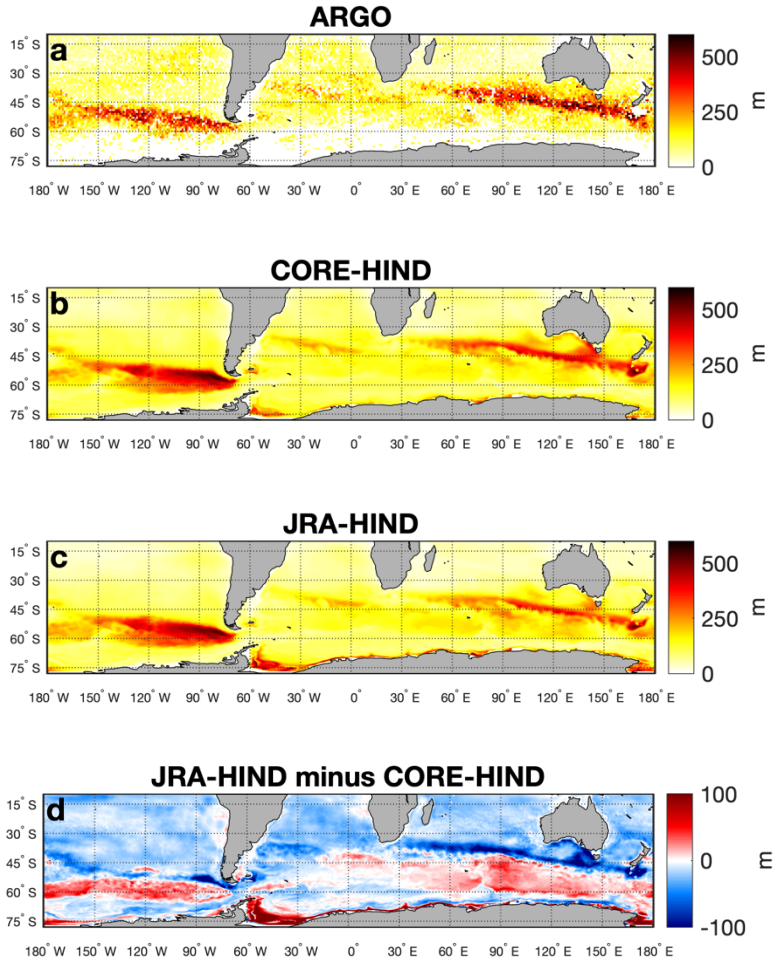

Fig. S2: Climatological September MLD (m) in **a)** ARGO (average between January 2000 and April 2018, Holte et al. 2017), **b)** CORE-HIND (1958-2009 average) **c)** JRA-HIND (1958-2018 average), **d)** difference between JRA-HIND and CORE-HIND. It should be noted that the MLD computed from ARGO data is based on a variable density threshold (Holte et al., 2017) and is therefore not strictly comparable to the simulated one.

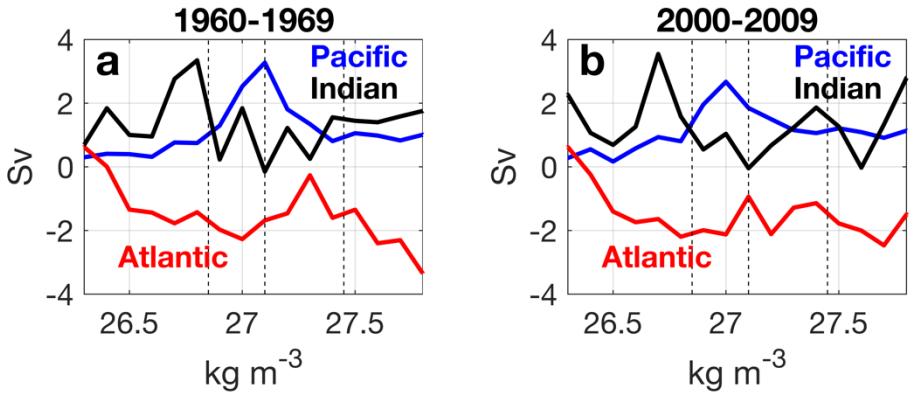

Fig. S3: Northward transport at 40°S in CORE-HIND averaged between years **a)** 1960-1969 and **b)** 2000-2009. Meridional velocities were integrated on 0.1 kg m^{-3} neutral density intervals and between 160°W-80°W (blue lines), 60°W-20°E (red lines), and 90°E-165°E (black lines). Dashed lines indicate the values of the CFC-12 inventory peaks in Fig. 3. It should be noted that, differently with respect to Fig. 3, the time average was performed before the integrations, that the sectors are smaller longitudinally, and that the neutral density bins are spaced 0.1 kg m^{-3} instead of 0.05 kg m^{-3}. The different computation is needed to obtain a relatively clean signal from the noisy velocity fields.

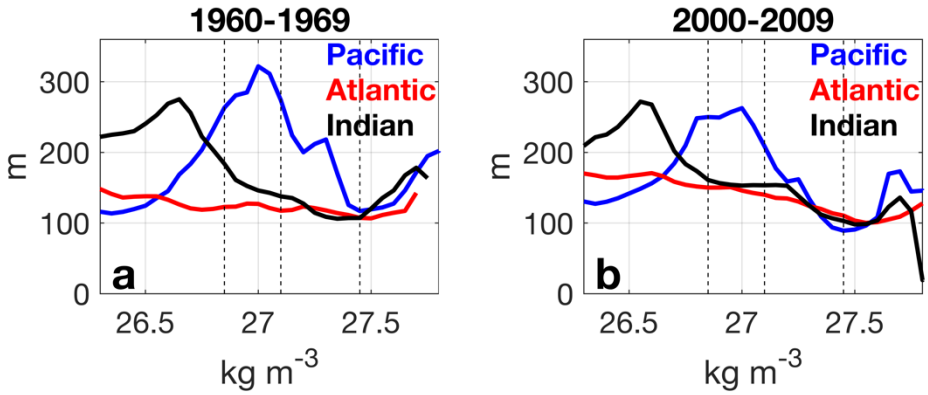

Fig. S4: September MLD in CORE-HIND averaged over the outcropping surfaces of 0.05 kg m^{-3} neutral density intervals, between 30°S-75°S and between 165°E-60°W (blue lines), 60°W-20°E (red lines), and 20°E-165°E (black lines). Shown are averages between years **(a)** 1960-1969 and **(b)** 2000-2009. Dashed lines indicate the values of the CFC-12 inventory peaks in Fig. 3. It should be noted that using the averaging method as in Fig. S3 yields substantially similar results.

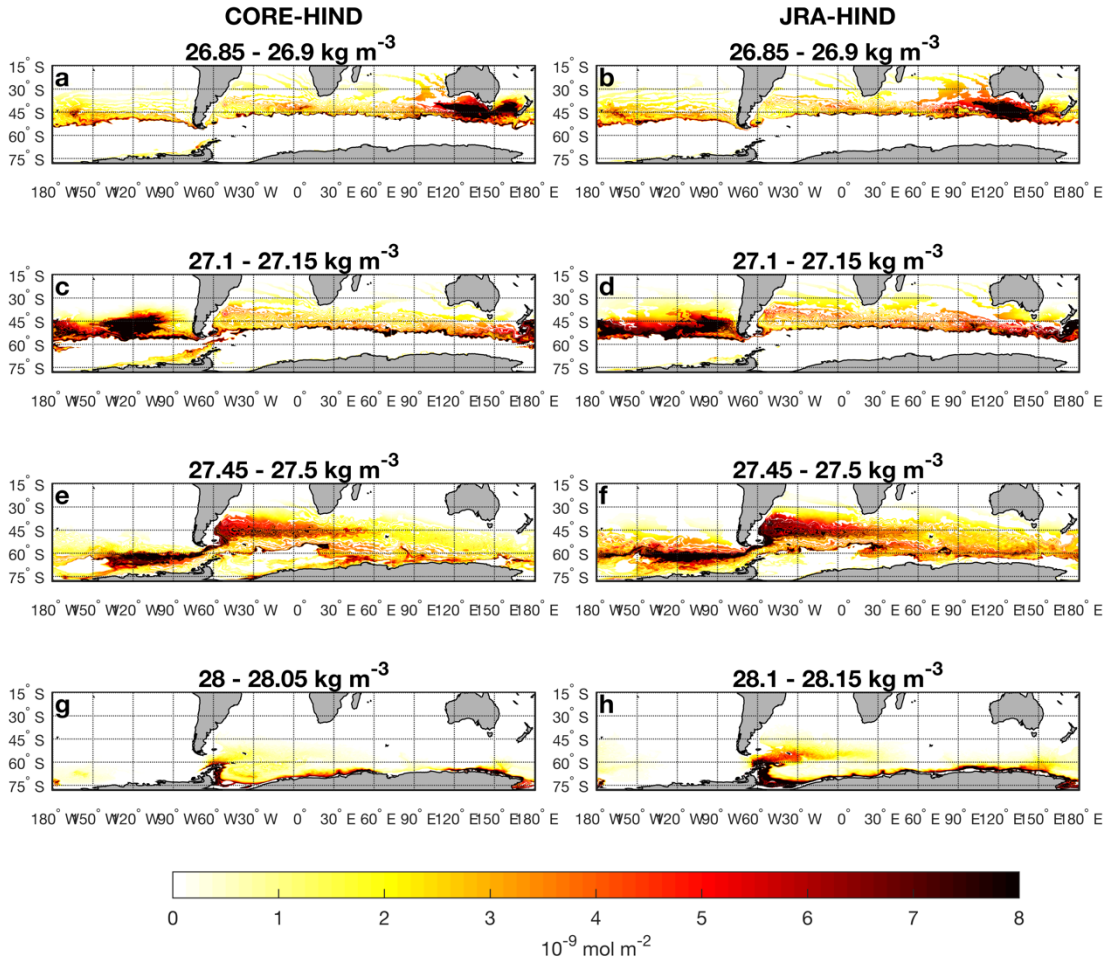

Fig. S5: CFC-12 inventories for year 1960 in **left)** CORE-HIND and in **right)** JRA-HIND integrated over **a,b)** 26.85-26.9 kg m^{-3}, **c,d)** 27.1-27.15 kg m^{-3}, **e,f)** 27.45 - 27.5 kg m^{-3}, **g)** 28 - 28.05 kg m^{-3} and **h)** 28.1 - 28.15 kg m^{-3} neutral density intervals. These density intervals have been selected based of CFC-12 inventory peaks in Fig. 3. It should be noted that CFC-12 inventories within the MLD are here included.

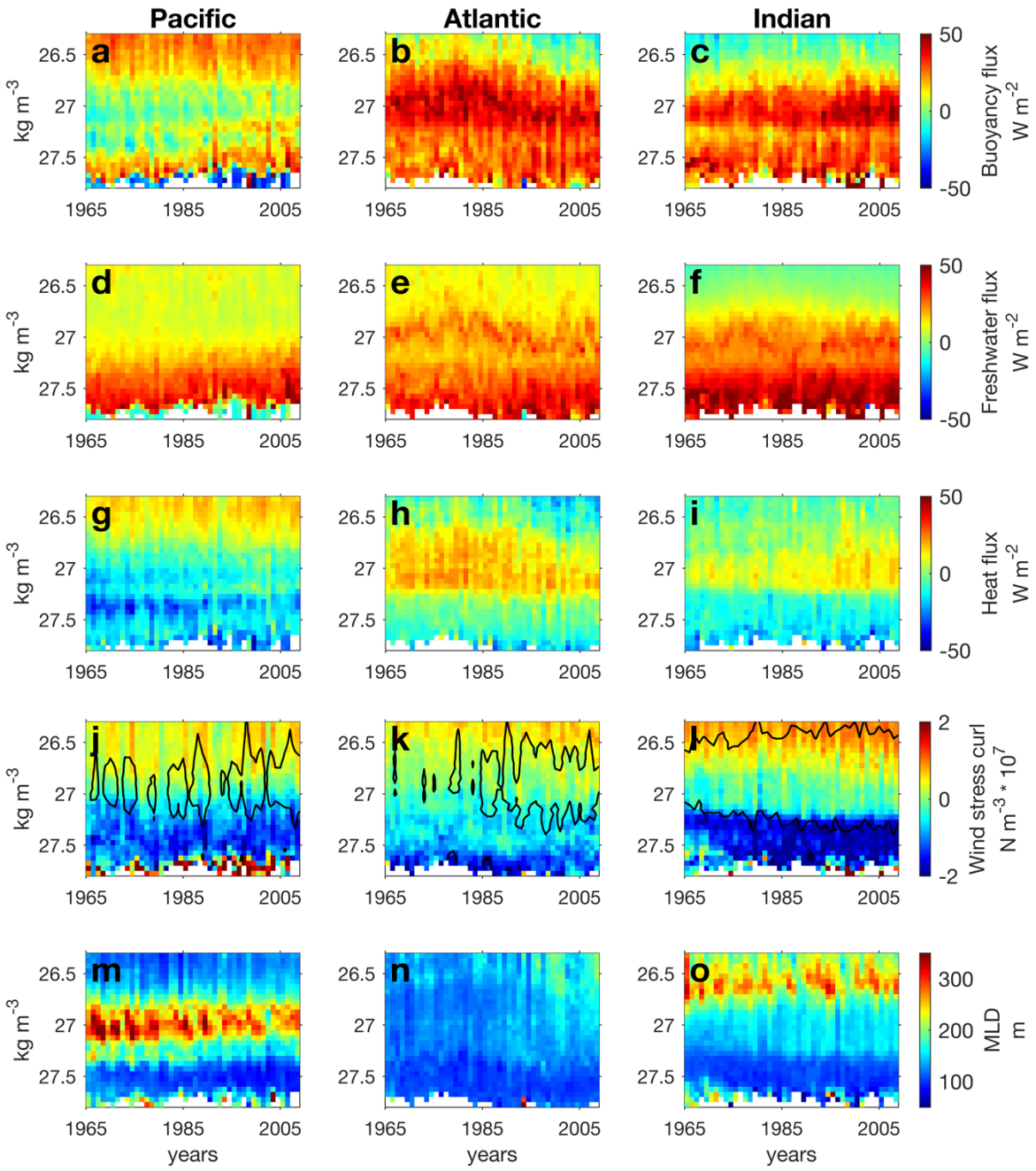

Fig. S6: **a-c)** Heat-equivalent air-sea buoyancy fluxes (positive indicates buoyancy gain) **d-f)** heat-equivalent net freshwater fluxes (positive indicates ocean freshwater gain), **g-i)** air-sea heat fluxes (positive indicates ocean heat gain), **j-l)** total wind stress (0.12 N m^{-2} contour) and wind stress curl (colors), and **m-o)** September MLD in CORE-HIND. The variables are averaged over outcropping surfaces of 0.05 kg m^{-3} neutral density intervals, between 30°S-75°S and over **left)** the Pacific sector (165°E-60°W), **middle)** the Atlantic sector (60°W-20°E), and **right)** the Indian sector (20°E-165°E). All quantities are annual averages except for the MLD.

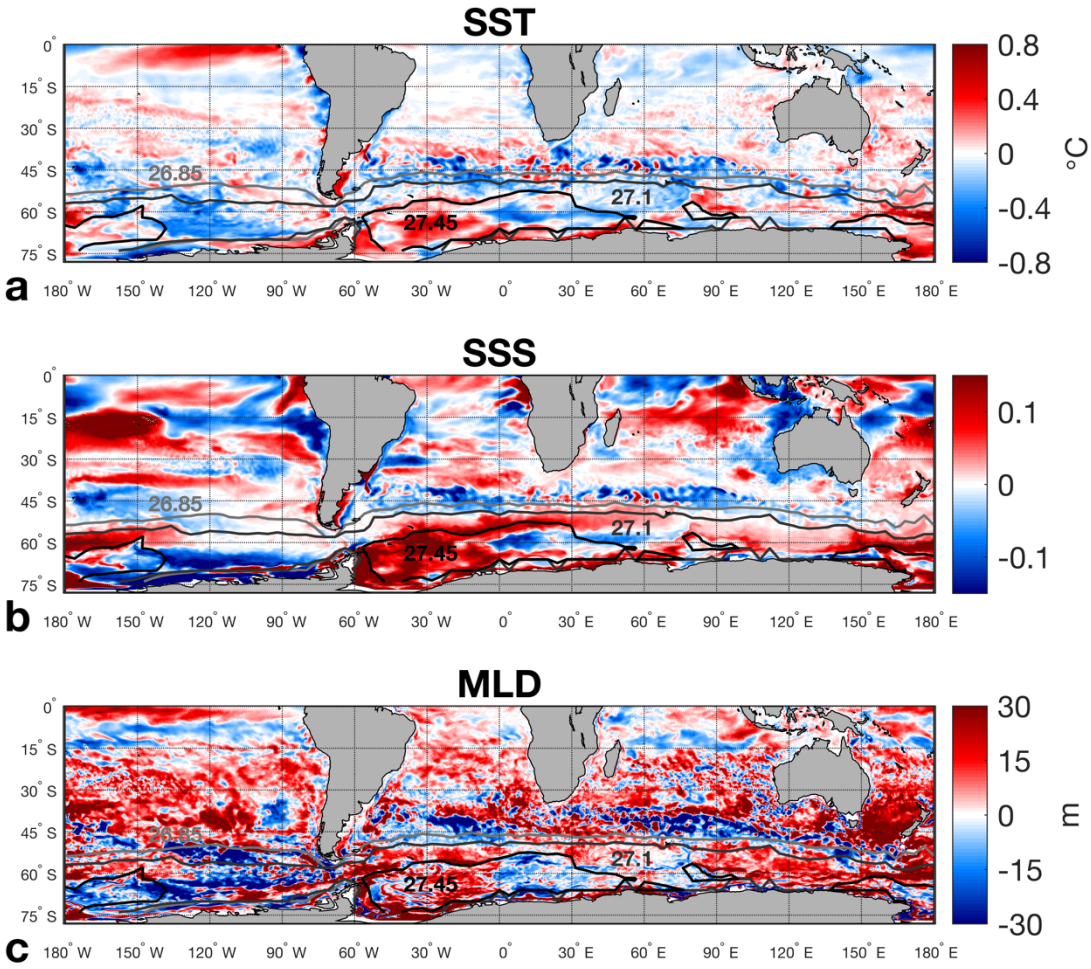

Fig. S7: Differences between CORE-WIND and CORE-CLIM of 1996-2005 averages of **a)** annually-averaged SST, **b)** annually-averaged SSS, and **c)** September MLD. Contours: selected neutral density surfaces at the surface ocean in CORE-WIND (smoothing applied).